



Impact of crystallinity on orbital torque generation in ferromagnets


Riko Fukunaga ¹, Satoshi Haku¹, Tenghua Gao ^{1,2,3}, Hiroki Hayashi ^{1,2}, and Kazuya Ando ^{1,2,4,*}

¹*Department of Applied Physics and Physico-Informatics, Keio University, Yokohama 223-8522, Japan*

²*Keio Institute of Pure and Applied Sciences, Keio University, Yokohama 223-8522, Japan*

³*State Key Laboratory of Advanced Technology for Materials Synthesis and Processing, Wuhan University of Technology, Wuhan 430070, China*

⁴*Center for Spintronics Research Network, Keio University, Yokohama 223-8522, Japan*

 (Received 14 November 2023; revised 6 March 2024; accepted 25 March 2024; published 15 April 2024)

We investigate the impact of crystallinity on the generation of orbital torques in Ni, which is predicted to exhibit the strongest orbital response among conventional 3d ferromagnetic metals. We show that the current-induced torques in Hf/Ni bilayers are primarily dominated by the orbital torque, arising from the orbital Hall effect in the Hf layer. We find that the orbital torque efficiency is enhanced by a factor of 2 when the stacking order of the Hf/Ni bilayer is altered. Through the examination of bulk and interfacial structural properties of the Ni and Hf layers, and by quantifying the torque efficiency in a symmetric Hf/Ni/Hf trilayer, we show that the orbital torque efficiency is strongly dependent on the crystallinity of the Ni layer. This dependence is in stark contrast to conventional spin-orbit torques, which arise from the spin Hall effect and are typically insensitive to the crystallinity of the ferromagnetic layer. These findings highlight the significant role of the crystalline structure of the ferromagnetic layer in its orbital response and illustrate the potential of crystal structure engineering in optimizing orbital torques.

DOI: [10.1103/PhysRevB.109.144412](https://doi.org/10.1103/PhysRevB.109.144412)

I. INTRODUCTION

The ability to electrically manipulate magnetization through current-induced spin-orbit torques offers a pathway to create energy-efficient, nonvolatile spintronic devices [1–5]. A primary mechanism for generating the spin-orbit torque is the spin Hall effect (SHE), which generates a spin current from a charge current through spin-orbit coupling [6,7]. The spin-orbit torque arising from the SHE has been shown to be significantly influenced by the crystalline structures in ferromagnetic-metal/nonmagnetic-metal (FM/NM) bilayers. In particular, the SHE in heavy metals, such as W and Ta, is strongly enhanced by altering the structure to the highly resistive phase, providing a route to improve the performance of spintronic devices [7]. In contrast, it has been demonstrated that the crystalline structure of the FM layer does not play an important role in generating the spin-orbit torque by the SHE [8].

The SHE has been predicted to emerge from the combined effects of the orbital Hall effect (OHE) and spin-orbit coupling [9]. The OHE is a phenomenon in which a charge current generates an orbital current, a flow of the orbital angular momentum of electrons. This phenomenon originates from the interband superpositions of Bloch states with different orbital characters induced by applying an electric field [10]. Recent studies have shown that the OHE can exert a torque on the magnetization in FM/NM structures, which is known as an orbital torque [11–19]. These studies have revealed the unique

features of the orbital transport and orbital torque, opening the field of orbitronics [20,21]. In solids, the dynamics of electronic orbital angular momentum is governed by crystal fields. Although this suggests that the orbital torque is sensitive to the crystal structure of FM/NM bilayers, the impact remains unclear.

In this paper, we show that the crystallinity of the FM layer has a significant impact on the orbital torque generation induced by the OHE. The evidence is obtained by investigating the current-induced torque in Hf/Ni and its inverted structure, where Ni has been shown to exhibit strong orbital response [12,14]. We show that this system allows us to probe the impact of the crystallinity of the Ni layer on the orbital response without significantly altering the electronic and structural properties of the Hf layer by inverting the stacking order. In contrast to the spin-orbit torque arising from the SHE, which is insensitive to the crystalline structure of the FM layer, we demonstrate that the orbital torque efficiency originating from the OHE is doubled by improving the crystallinity of the Ni layer. This result illustrates the strong impact of the crystallinity of a FM on the orbital torque, providing insights for deeper understanding of the orbital response and transport.

II. EXPERIMENTAL METHODS

We investigated the current-induced torque using spin torque ferromagnetic resonance (ST-FMR) for the Hf(t_{Hf})/Ni(12 nm), Ni(12 nm)/Hf(t_{Hf}), Hf(10 nm)/Ni(t_{Ni}), and Ni(t_{Ni})/Hf(10 nm) bilayers, where the numbers in parentheses represent the thickness. The films were deposited on SiO₂/Si substrates by radio frequency (rf) magnetron

*ando@appi.keio.ac.jp

sputtering in an Ar atmosphere, where the base pressure was better than 6×10^{-6} Pa. During the sputtering of the Hf layer, a linear shutter was used to vary the thickness. The Hf(Ni) thickness variation across each device is 0.06(0.02) nm. To protect the film surface from oxidation, we sputtered a 4-nm-thick SiO₂ film. The films were patterned into $150 \mu\text{m} \times 10 \mu\text{m}$ stripes by photolithography and Ar ion milling. On the edges of the stripes, Au(300 nm)/Ti(3 nm) electrodes were sputtered for the rf current application.

For the ST-FMR measurement, an rf current with a power of $P = 100$ mW and a frequency of f was passed through the device, and a direct current (dc) voltage, V_{dc} , was measured while sweeping an in-plane external magnetic field H applied at an angle θ_H with respect to the applied rf current. The rf current generates both dampinglike (DL) and fieldlike (FL) effective fields, H_{DL} and H_{FL} , as well as an Oersted field H_{Oe} . These fields drive the magnetization precession in the Ni layer at the FMR, which results in the oscillation of the device resistance due to the anisotropic magnetoresistance (AMR). The mixing of the oscillatory resistance and the oscillatory applied current produces a dc voltage. The dc voltage was measured using a bias tee and a nanovoltmeter at room temperature.

III. RESULTS AND DISCUSSION

A. Spin-torque ferromagnetic resonance

In Fig. 1(a), we show the ST-FMR spectra measured for the Hf(10 nm)/Ni(12 nm)/SiO₂-substrate at $\theta_H = 45^\circ$. To determine the DL-torque efficiency [14,22],

$$\xi_{\text{DL}}^E = \zeta \frac{2e}{\hbar} \mu_0 M_s t_{\text{Ni}} \frac{H_{\text{DL}}}{E}, \quad (1)$$

we fit the measured ST-FMR signal using the sum of the symmetric and antisymmetric functions [23]: $V_{\text{dc}} = SW^2/[(\mu_0 H - \mu_0 H_{\text{res}})^2 + W^2] + A[W(\mu_0 H - \mu_0 H_{\text{res}})]/[(\mu_0 H - \mu_0 H_{\text{res}})^2 + W^2]$, where \hbar is the reduced Planck constant, M_s is the saturation magnetization, t_{Ni} is the thickness of the Ni layer, E is the applied electric field, H_{res} is the FMR field, and W is the linewidth. $\zeta = 1$ for the NM/FM structure and $\zeta = -1$ for the FM/NM structure. The polarization direction of the orbital current injected into the Ni layer is opposite between the Hf/Ni and Ni/Hf bilayers. In fact, the sign of H_{DL} determined by the ST-FMR is opposite between the Hf/Ni and Ni/Hf bilayers. In contrast, the signs of the spin and orbital Hall conductivities of the Hf layer are independent of the stacking order. By introducing the factor of $\zeta = \pm 1$, the DL-torque efficiency ξ_{DL}^E is defined such that its sign is determined by the sign of the dominant mechanism of the torque generation, i.e., the SHE or OHE, of the Hf layer.

In the V_{dc} signal, the DL effective field H_{DL} is proportional to the symmetric component S as [24]

$$\mu_0 H_{\text{DL}} = \frac{2\sqrt{2}SW}{I_{\text{rf}} \Delta R_{\text{AMR}}} \frac{2\mu_0 H_{\text{res}} + \mu_0 M_{\text{eff}}}{\mu_0 H_{\text{res}} + \mu_0 M_{\text{eff}}} \sqrt{1 + \frac{\mu_0 M_{\text{eff}}}{\mu_0 H_{\text{res}}}}, \quad (2)$$

where ΔR_{AMR} is the resistance change of the device due to the AMR. I_{rf} is the rf current flowing in the device, which is determined by monitoring the resistance change induced by the Joule heating due to the application of the rf current [24–26].

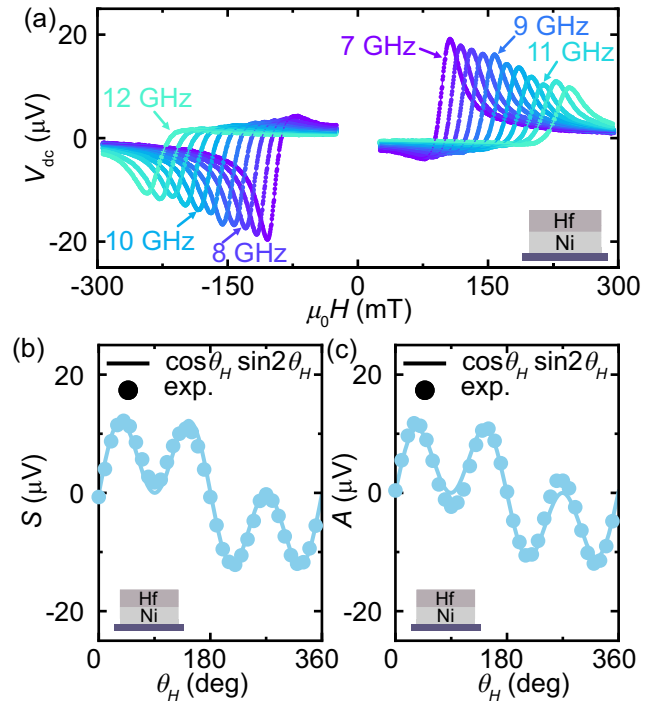


FIG. 1. (a) ST-FMR spectra for the Hf(10 nm)/Ni(12 nm) bilayer at $\theta_H = 45^\circ$. The frequency f was varied from 7 to 12 GHz. The solid circles and curves represent the experimental data and the fitting results, respectively. In-plane magnetic field angle θ_H dependence of (b) the symmetric component S and (c) the antisymmetric component A for the Hf(10 nm)/Ni(12 nm) bilayer. The solid circles are the experimental data. The solid curve is the fitting result using a function proportional to $\cos \theta_H \sin 2\theta_H$.

The antisymmetric component A is proportional to the sum of the FL effective field H_{FL} and the Oersted field H_{Oe} . As shown in Figs. 1(b) and 1(c), we find $S \propto \cos \theta_H \sin 2\theta_H$ and $A \propto \cos \theta_H \sin 2\theta_H$, consistent with the model of the ST-FMR [24]. This result indicates that an out-of-plane Oersted field is negligible, showing that the applied rf current flows uniformly in the device.

Figure 2(a) shows Hf-layer-thickness t_{Hf} dependence of ξ_{DL}^E for the Hf/Ni bilayer. This result shows that the sign of the DL torque is positive and the DL torque efficiency increases with increasing t_{Hf} . The t_{Hf} dependent variation in ξ_{DL}^E shows that the DL torque originates from the current flow in the bulk of the Hf layer, indicating that the observed torque can be attributed to the SHE or the OHE. We note that the sign of the SHE is negative, while that of the OHE is positive in Hf [27]. This indicates that the DL torque is dominated by the OHE in the Hf layer in the Hf/Ni bilayer. This result aligns with previous studies on the current-induced torque generated by Hf [28–30]. In the devices used in the previous studies, the FM layer is CoFeB. In such devices, the SHE dominates the current-induced torque arising from the current flow in the Hf layer. In contrast, our results indicate that the OHE provides the dominant contribution to the torque when the FM layer is Ni. The difference in the roles of the SHE and OHE between the CoFeB-based and Ni-based devices is consistent with the fact that the orbital response strongly depends on the electronic structure of the FM layer [31].

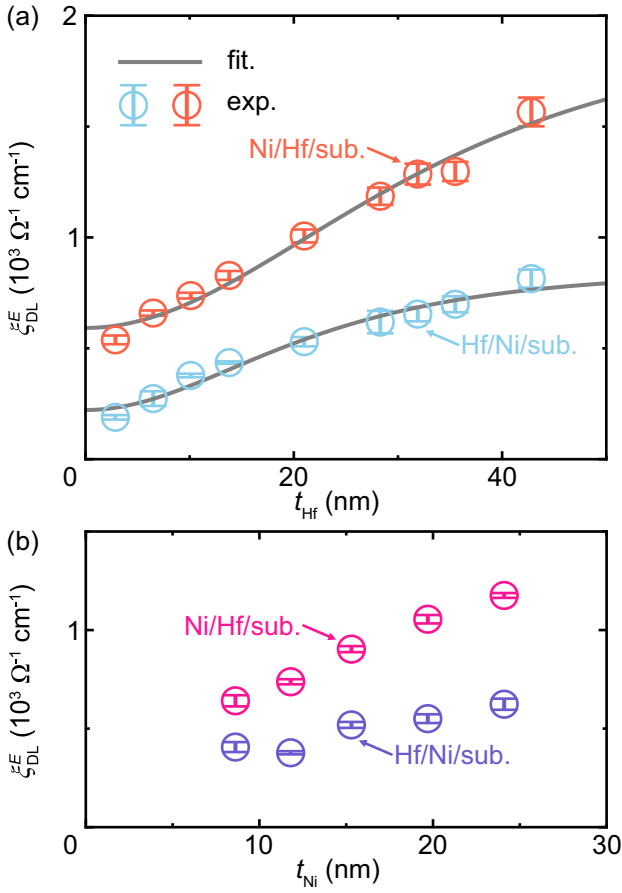


FIG. 2. (a) Hf-layer-thickness t_{Hf} dependence of the DL torque efficiency ξ_{DL}^E for the Hf(t_{Hf})/Ni(12 nm) bilayer (blue) and the Ni(12 nm)/Hf(t_{Hf}) bilayer (red). (b) Ni-layer-thickness t_{Ni} dependence of the DL torque efficiency ξ_{DL}^E for the Hf(10 nm)/Ni(t_{Ni}) bilayer (blue) and the Ni(t_{Ni})/Hf(10 nm) bilayer (red). The open circles are the experimental data. The solid curves are the fitting results.

In fact, a similar conclusion has been obtained for Ta/FM bilayers; the current-induced torque is dominated by the SHE in a Ta/CoFeB bilayer, whereas it is dominated by the OHE in a Ta/Ni bilayer due to the stronger orbital response of Ni compared to CoFeB [12].

To verify our assumption that the observed torque in the Hf/Ni bilayer is dominated by the OHE in the Hf layer, we investigated the DL torque efficiency by varying the thickness of the Ni layer t_{Ni} , as shown in Fig. 2(b). In the Ni layer, the behavior of spin and orbital transport is fundamentally different. When a spin current is injected into a FM, the spin current decays within 1 nm due to spin dephasing. In contrast, an orbital current can propagate over much longer distances than the spin dephasing length [32]. Because of the short spin dephasing length, ξ_{DL}^E should be independent of the FM layer thickness within the range studied in Fig. 2(b) when the SHE is dominant. However, Fig. 2(b) shows that ξ_{DL}^E increases with t_{Ni} , which is consistent with the long-range nature of orbital transport in FMs [14,15,17,19,32,33]. This result provides further evidence that the DL torque in the Hf/Ni bilayer is dominated by the OHE.

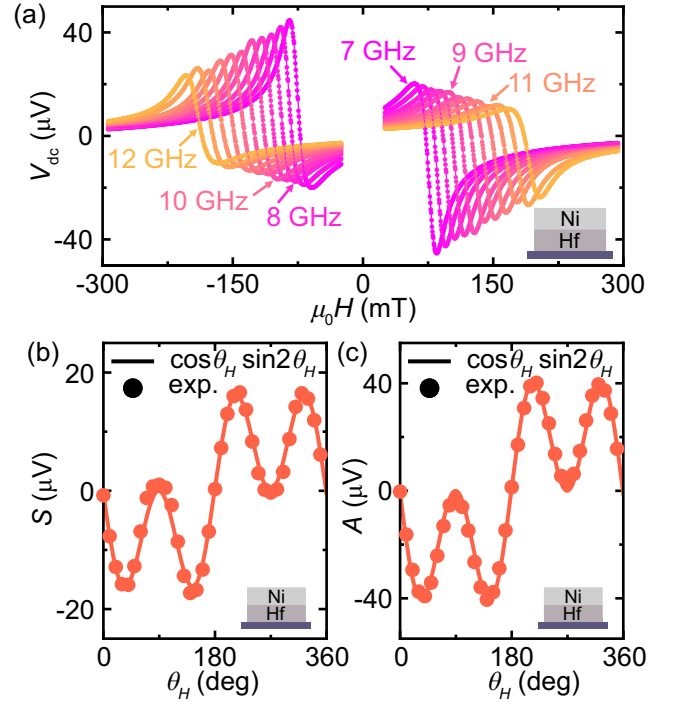


FIG. 3. (a) ST-FMR spectra for the Ni(12 nm)/Hf(10 nm) bilayer at $\theta_H = 45^\circ$. The frequency f was varied from 7 to 12 GHz. The solid circles and curves represent the experimental data and the fitting results, respectively. In-plane magnetic field angle θ_H dependence of (b) the symmetric component S and (c) the antisymmetric component A for the Ni(12 nm)/Hf(10 nm) bilayer. The solid circles are the experimental data. The solid curve is the fitting result using a function proportional to $\cos\theta_H \sin 2\theta_H$.

We analyze the t_{Hf} dependence of ξ_{DL}^E based on a spin and orbital drift-diffusion model [15]. We assume that the spin-orbital interconversion is sufficiently weak in the Hf layer such that $\lambda_S \ll \lambda_L$, λ_{LS} , where $\lambda_{L(S)}$ is the spin (orbital) diffusion length, and λ_{LS} is a parameter that characterizes the strength of the spin-orbital interconversion. In the limit of a transparent interface [23], the orbital torque efficiency under this assumption is proportional to $1 - \text{sech}(t_{Hf}/\lambda_L)$ as $\xi_{DL}^E = \xi_{DL,L}^E [1 - \text{sech}(t_{Hf}/\lambda_L)]$, where $\xi_{DL,L}^E$ characterizes the strength of the orbital torque. The experimentally determined t_{Hf} dependence of ξ_{DL}^E suggests that there is a contribution to the DL torque that is independent of t_{Hf} . To take into account this contribution, we fit the experimental data using

$$\xi_{DL}^E = \xi_{DL,L}^E \left[1 - \text{sech}\left(\frac{t_{Hf}}{\lambda_L}\right) \right] + C, \quad (3)$$

where C represents the t_{Hf} -independent contribution to the DL torque. The independence of C on t_{Hf} suggests its interfacial nature, which can be attributed to interfacial spin-orbit torques due to interfacial Rashba-type spin-orbit coupling. By fitting the experimental data shown in Fig. 2(a) using Eq. (3), we obtain $\xi_{DL,L}^E = 622 \pm 62 \Omega^{-1} \text{cm}^{-1}$, $\lambda_L = 15.6 \pm 2.8 \text{ nm}$, and $C = 222 \pm 32 \Omega^{-1} \text{cm}^{-1}$ for the Hf/Ni bilayer. The extracted characteristic length λ_L is clearly larger than the spin diffusion length of Hf, around 2 nm [30,34], consistent with recent

TABLE I. Comparison of the Hf/Ni/SiO₂-substrate and Ni/Hf/SiO₂-substrate devices. The DL torque efficiency $\xi_{\text{DL,L}}^E$ of the Ni/Hf bilayer is larger than that of the Hf/Ni bilayer by a factor of 2. The resistivity of the Ni(12 nm) layer, ρ_{Ni} (12 nm), and that of the Hf layer, ρ_{Hf} (t_{Hf}), and the crystallite size of the Ni(12 nm) layer, D_{Ni} , in the Hf/Ni and Ni/Hf bilayers are summarized. The t_{Hf} -dependent resistivity $\rho_{\text{Hf}}(t_{\text{Hf}})$ was determined by fitting the measured resistivity of the Hf layer using $\rho_{\text{Hf}}(t_{\text{Hf}}) = \rho_{\text{bulk}} + at_{\text{Hf}}^{-1}$, where ρ_{Hf} is the resistivity in the bulk limit and at_{Hf}^{-1} represents the resistivity due to the surface scattering.

Device	$\xi_{\text{DL,L}}^E$ ($\Omega^{-1}\text{cm}^{-1}$)	ρ_{Ni} (12 nm) ($\mu\Omega\text{cm}$)	$\rho_{\text{Hf}}(t_{\text{Hf}})$ ($\mu\Omega\text{cm}$)	D_{Ni} (nm)
SiO ₂ /Hf/Ni/SiO ₂ substrate	622 ± 62	19.6	$79.1 + 5.86 \times 10^{-7} t_{\text{Hf}}^{-1}$	5.19 ± 0.13
SiO ₂ /Ni/Hf/SiO ₂ substrate	1352 ± 213	14.4	$91.6 + 1.58 \times 10^{-7} t_{\text{Hf}}^{-1}$	8.41 ± 0.05

reports that the orbital diffusion length is longer than the spin diffusion length [14,32].

Our finding is that the DL torque efficiency $\xi_{\text{DL,L}}^E$ is enhanced by reversing the stacking order of the Hf/Ni/SiO₂-substrate structure. The ST-FMR result for the inverted Ni(12 nm)/Hf(10 nm)/SiO₂-substrate structure is summarized in Fig. 3, and the determined values of ξ_{DL}^E are shown in Fig. 2. From the result shown in Fig. 2(a), we obtain $\xi_{\text{DL,L}}^E = 1352 \pm 213 \Omega^{-1}\text{cm}^{-1}$, $\lambda_L = 23.6 \pm 4.1$ nm, and $C = 592 \pm 34 \Omega^{-1}\text{cm}^{-1}$ for the Ni/Hf bilayer. This result demonstrates that the DL torque efficiency of the OHE, $\xi_{\text{DL,L}}^E$, is doubled by reversing the stacking order of the Hf/Ni bilayer.

To reveal the origin of the enhancement of the orbital torque efficiency, we express the orbital torque efficiency as $\xi_{\text{DL,L}}^E [1 - \text{sech}(t_{\text{Hf}}/\lambda_L)] = \eta_{\text{FM}} T_{\text{int}} \sigma_{\text{OHE}}$, where T_{int} and σ_{OHE} are the interfacial orbital transparency and the orbital Hall conductivity of the Hf layer, respectively. Here, η_{FM} represents the strength of the orbital response in the FM layer, which arises from a combined action of the spin-orbit coupling and spin-exchange coupling in the FM layer [11]. To obtain insight into σ_{OHE} in the Hf/Ni and Ni/Hf bilayers, we determined the resistivity ρ_{Hf} of the Hf layer in the Hf/Ni and Ni/Hf bilayers (see Table I). This result shows that the Hf layer is in the moderately dirty regime in both the Hf/Ni and Ni/Hf bilayers, suggesting that the OHE in the Hf layer is dominated by the intrinsic mechanism. Since the intrinsic orbital Hall conductivity is predicted to be independent of ρ_{Hf} , we assume that σ_{OHE} is nearly identical between the Hf/Ni and Ni/Hf bilayers. This indicates that the difference in the orbital torque efficiency between the Hf/Ni and Ni/Hf bilayers can be attributed to a difference in $\eta_{\text{FM}} T_{\text{int}}$.

B. Materials characterization

To clarify the origin of the difference in the orbital torque efficiency, or $\eta_{\text{FM}} T_{\text{int}}$, between the Hf/Ni and Ni/Hf bilayers, we examined the crystalline structure of the Hf and Ni layers by conducting x-ray diffraction (XRD) measurements for the Hf(28 nm)/Ni(12 nm) bilayer and the Ni(12 nm)/Hf(28 nm) bilayer, as shown in Fig. 4. As shown in Fig. 4(a), the XRD patterns of the Hf layer demonstrate that the Hf layer is a hexagonal closed-packed (hcp) structure in both the Hf/Ni and Ni/Hf bilayers. This result also shows that the XRD patterns are almost identical between the bilayers, confirming that the crystallinity of the Hf layer is insensitive to the stacking order. In contrast, the XRD patterns of the Ni layer in the different films are strongly dependent on the stacking order. The XRD patterns shown in Fig. 4(b) indicate that the

Ni layer is a face-centered cubic (fcc) structure in the Hf/Ni and Ni/Hf films.

From the XRD results, we estimate the crystallite size D using the Scherrer equation [35–37],

$$D = \frac{K\lambda}{\beta \cos \theta}, \quad (4)$$

where $K = 0.9$ is the Scherrer constant, λ is the x-ray wavelength, β is the full width at half maximum of the XRD peaks in radians, and θ is the Bragg angle. Here, D for the (hkl) peak represents the volume-weighted mean column length, that is, a mean crystallite size in the direction perpendicular to the (hkl) plane [37], where hkl are the Miller indices. The crystallite size of the Hf layers is almost identical in the Hf/Ni and Ni/Hf bilayers; we obtain $D_{\text{Hf}} = 11.61 \pm 0.05$ nm and $D_{\text{Hf}} = 11.28 \pm 0.04$ nm for the Hf(28 nm)/Ni(12 nm) and Ni(12 nm)/Hf(28 nm) bilayers, respectively, from the Hf(0002) peaks shown in Fig. 4(a). Here, the error of D estimated from the Scherrer equation is the standard error of the Gaussian fitting. In contrast to the almost identical crystallite size of Hf layers in the different films, the XRD

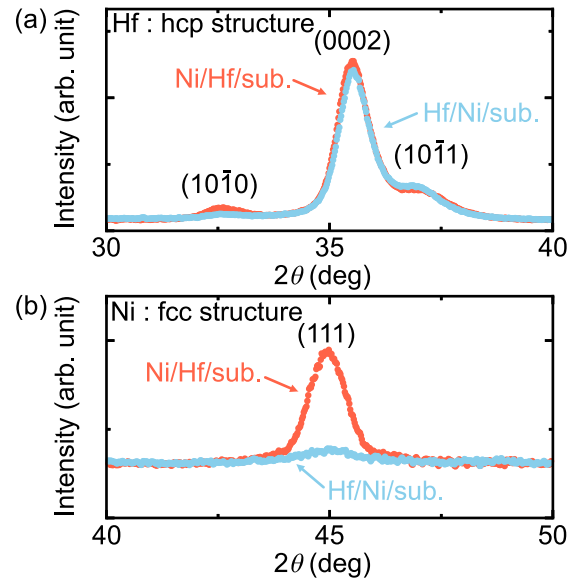


FIG. 4. (a) XRD patterns for the Hf(28 nm) layer in the Hf(28 nm)/Ni(12 nm) bilayer (blue) and the Ni(12 nm)/Hf(28 nm) bilayer (red). The XRD patterns show that the Hf layer is a hexagonal closed-packed (hcp) structure. (b) XRD patterns for the Ni(12 nm) layer in the Hf(28 nm)/Ni(12 nm) bilayer (blue) and the Ni(12 nm)/Hf(28 nm) bilayer (red). The XRD patterns show that the Ni layer is a face-centered cubic (fcc) structure.

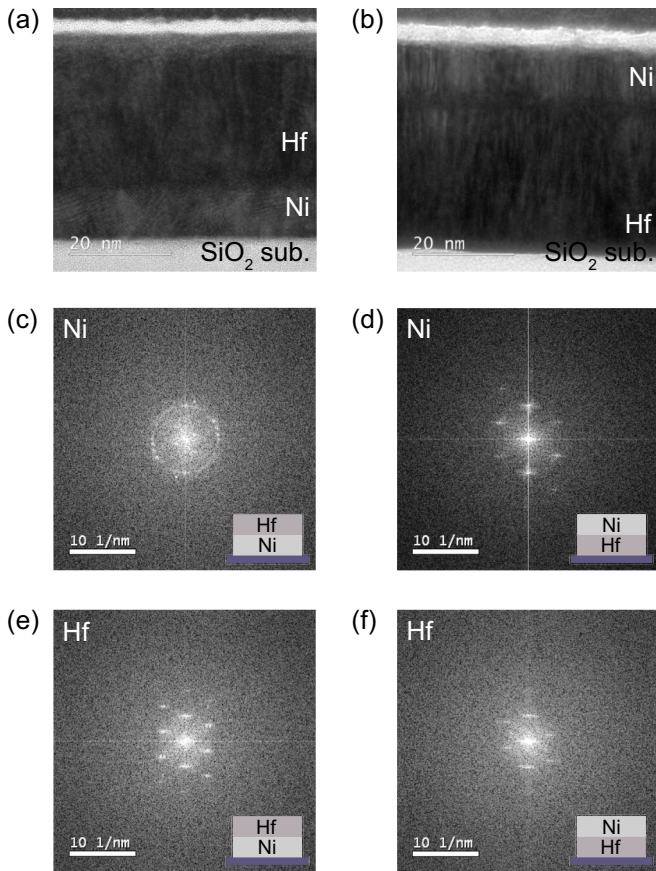


FIG. 5. Cross-sectional transmission electron microscope images of the (a) Hf/Ni and (b) Ni/Hf bilayers. Fast Fourier transform patterns for the Ni layers of the (c) Hf/Ni and (d) Ni/Hf bilayers, and the Hf layers of the (e) Hf/Ni and (f) Ni/Hf bilayers.

results demonstrate that the crystallite size of the Ni layer strongly depends on the stacking order; the crystallite size estimated from the Ni(111) peak is $D_{\text{Ni}} = 5.19 \pm 0.13$ nm for the Hf(28 nm)/Ni(12 nm) bilayer, and $D_{\text{Ni}} = 8.41 \pm 0.05$ nm for the Ni(12 nm)/Hf(28 nm) bilayer, showing better crystallinity of the Ni layer in the Ni/Hf bilayer compared to that in the Hf/Ni bilayer.

The degree of texture can be quantified by estimating the peak height ratio from a single XRD pattern. For the Hf layer, the peak height ratio of $A(10\bar{1}1)/A(0002)$ is 0.32 for the Hf/Ni bilayer and 0.28 for the Ni/Hf bilayer. The obtained results are very close, indicating a similar crystallinity of the Hf layers in the Hf/Ni and Ni/Hf bilayers. For the Ni layer, the clear difference in the strength of the XRD peaks suggests a higher degree of (111) texture in the Ni/Hf bilayer compared to the Hf/Ni bilayer. However, it is challenging to quantify the degree of texture from the XRD patterns because only one XRD peak is observed. Since the XRD peak intensity depends on many factors during the measurements, such as the small tilting angle of the film surface to the sample holder, it is inappropriate to directly compare the XRD peak intensity from the XRD patterns of each sample. Thus, to further study the microstructure of the Ni and Hf layers, we have performed the cross-sectional transmission electron microscope (TEM)

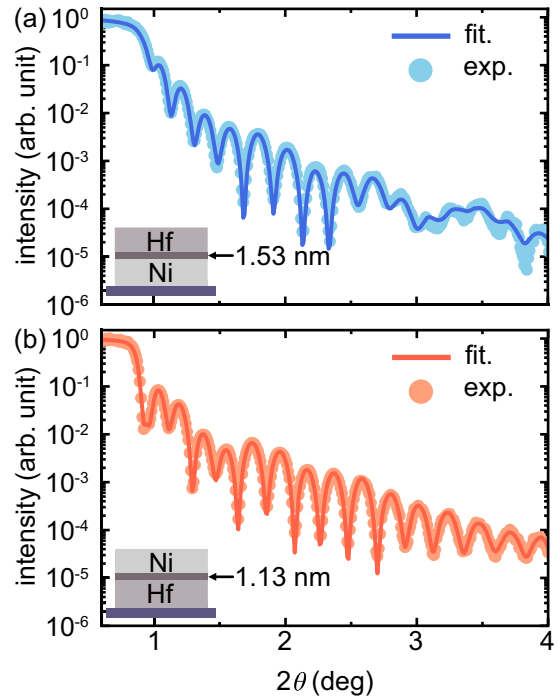


FIG. 6. XRR profiles for (a) the Hf(28 nm)/Ni(12 nm) bilayer and (b) the Ni(12 nm)/Hf(28 nm) bilayer. The solid circles and curves are the experimental data and the fitting results, respectively. Schematic illustration of the structure with the thickness of the intermixing layer is also shown in the inset.

observations on the Hf/Ni and Ni/Hf bilayers, as shown in Figs. 5(a) and 5(b), respectively.

From the TEM results, the structures of the Ni and the Hf layer are characterized using the fast Fourier transform (FFT) patterns. As shown in Fig. 5(c), the FFT pattern of the Ni layer in the Hf/Ni bilayer reveals a diffraction ring, indicating the presence of small crystallites of Ni without a preferred crystallographic orientation during the thin film growth. This suggests that the polycrystalline grains are randomly distributed in the Ni layer. In contrast, as shown in Fig. 5(d), the FFT pattern of the Ni layer in the inverted structure (Ni/Hf) shows strong diffraction spots along the film normal direction from {111} plane diffraction, which confirms a strong Ni (111) texture. This indicates that, besides the {111} planes, nearly no other crystallographic facets are parallel to the film surface. These results are consistent with the XRD results, where a vanishingly small Ni (111) peak in the Hf/Ni bilayer and a strong Ni (111) peak in the Ni/Hf bilayer are observed, supporting a higher degree of (111) texture in the Ni layer of the Ni/Hf bilayer compared to the Hf/Ni bilayer. For the Hf layers, the FFT patterns show strong diffraction spots along the film normal direction in both the Ni/Hf and Hf/Ni bilayers, indicating a strong crystallographic texture. These results are also consistent with the XRD results.

We also characterize the interfaces by x-ray reflectivity (XRR) for the Hf(28 nm)/Ni(12 nm) and Ni(12 nm)/Hf(28 nm) bilayers, as shown in Figs. 6(a) and 6(b). By fitting the data based on the Levenberg-Marquardt method, we obtain the thickness of the intermixing layer as 1.53 nm at the Hf/Ni interface and 1.13 nm at the Ni/Hf

interface. This result suggests that the intermixing-layer thickness, as well as the crystallinity of the Ni layer, is different between the Hf/Ni and Ni/Hf bilayers. To study the impact of the intermixing-layer thickness on the orbital torque generation, we also measured the DL torque efficiency for a Hf/Ni/Hf film (see Appendix). The result shows that T_{int} is almost identical between the top Hf/Ni and bottom Ni/Hf interfaces, suggesting that a slight difference in the thickness of the intermixing layer does not significantly alter the interfacial orbital transparency T_{int} . However, it cannot be concluded that T_{int} is nearly identical between the Hf/Ni and Ni/Hf bilayers because the microstructure of the Ni layer is clearly different between the Hf/Ni and Ni/Hf bilayers, while the nearly identical T_{int} is demonstrated between the Hf/Ni and Ni/Hf interfaces with the well-crystalline Ni layer. Rather, these observations imply that the primary factor potentially leading to a difference in T_{int} between the Hf/Ni and Ni/Hf bilayers could be the distinct microstructures of the Ni layer rather than the thickness of the intermixing layer. In the present study, we assume that both η_{FM} and T_{int} are influenced by the crystallinity of the Ni layer. Identifying which parameter is more sensitive to the crystallinity of the Ni layer remains challenging at this stage, and we leave this for future study.

The above results demonstrate the strong impact of the crystallinity of the FM layer on the generation of the orbital torque induced by the OHE. This result is clearly different from the generation of the spin-orbit torque by the SHE. A previous study has demonstrated that the spin-orbit torque originating from the SHE is insensitive to the crystallinity of the FM layer in FM/NM structures [8]. These observations are consistent with a theoretical prediction that the spin injection is less susceptible to the crystalline structure, while the orbital injection depends strongly on the crystallinity, which determines the orbital hybridization [32]. Here, Fig. 2(a) also shows a clear difference in the t_{Hf} -independent contribution of ξ_{DL}^E , C : $C = 222 \Omega^{-1}\text{cm}^{-1}$ in the Hf/Ni bilayer and $C = 592 \Omega^{-1}\text{cm}^{-1}$ in the Ni/Hf bilayer. This result suggests that the interfacial Rashba effect is more pronounced in the Ni/Hf bilayer than in the Hf/Ni bilayer. This result is consistent with a previous report, which suggests that the emergence of the (111) structure in the FM layer enlarges the interfacial symmetry breaking and consequently enhances the interfacial Rashba effect [8].

IV. CONCLUSIONS

In conclusion, we have investigated the current-induced torque in the Hf/Ni and Ni/Hf bilayers using the ST-FMR. We found that the DL torque efficiency in the Hf/Ni and Ni/Hf bilayers increases with increasing the Hf thickness. The sign of the observed torque suggests that the OHE is the dominant mechanism of the torque generation. We also found that the torque efficiency increases by increasing the Ni thickness, providing evidence that the torque is dominated by orbital currents. Our results show that the orbital torque efficiency of the Ni/Hf bilayer is larger than that of the Hf/Ni bilayer by a factor of two, which is attributed to the difference in the crystallinity of the Ni layer. A recent experiment has shown that the orbital torque depends on the interface crystallinity

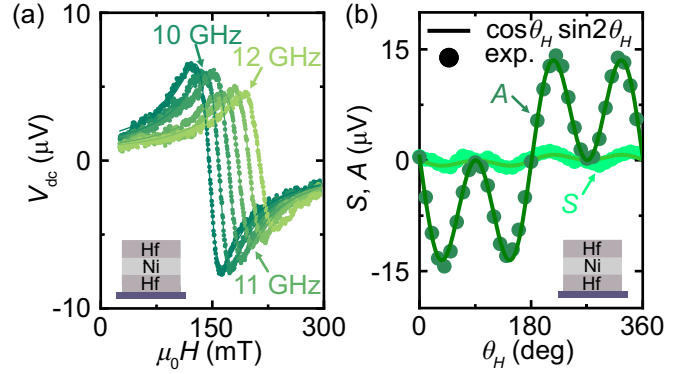


FIG. 7. (a) ST-FMR spectra for the Hf(10 nm)/Ni(12 nm)/Hf(10 nm) trilayer at $\theta_H = 45^\circ$. The frequency f was varied from 9.5 GHz to 12 GHz. The solid circles and curves represent the experimental data and the fitting results, respectively. (b) In-plane magnetic field angle θ_H dependence of the symmetric component S and the antisymmetric component A . The solid circles are the experimental data. The solid curves are the fitting result using functions proportional to $\cos\theta_H \sin 2\theta_H$.

[38]. Our results demonstrate that the bulk crystallinity of the FM layer, as well as the interface crystallinity, plays an important role in the orbital response. This is consistent with the fact that the orbital dynamics is governed by crystal fields in solids.

ACKNOWLEDGMENTS

This work was supported by JSPS KAKENHI (Grants No. 22H04964, No. 20H00337, and No. 20H02593), Spintronics Research Network of Japan (Spin-RNJ), and MEXT Initiative to Establish Next-generation Novel Integrated Circuits Centers (X-NICS) (Grant No. JPJ011438).

APPENDIX

We measured the ST-FMR for a $\text{SiO}_2(4 \text{ nm})/\text{Hf}(10 \text{ nm})/\text{Ni}(12 \text{ nm})/\text{Hf}(10 \text{ nm})/\text{SiO}_2$ -substrate structure, as shown

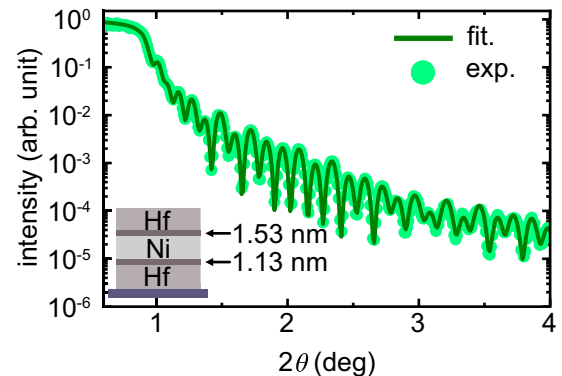


FIG. 8. XRR profiles for the Hf(28 nm)/Ni(12 nm)/Hf(28 nm) trilayer. The solid circles and curves are the experimental data and the fitting results, respectively. Schematic illustration of the structure with the thicknesses of the intermixing layers is also shown in the inset.

in Fig. 7. From this result, we obtain the DL torque efficiency of the symmetric Hf/Ni/Hf trilayer as $|\xi_{\text{DL}}^E| = 16 \Omega^{-1}\text{cm}^{-1}$. The vanishingly small ξ_{DL}^E indicates the cancellation of the torques from the top Hf/Ni and bottom Ni/Hf layers, demonstrating that $T_{\text{int}}\sigma_{\text{OHE}}$ is almost identical between the top Hf/Ni and bottom Ni/Hf layers. This result shows that T_{int} is also almost identical between the Hf/Ni and Ni/Hf interfaces because of the nearly identical

σ_{OHE} of the top and bottom Hf layers. Figure 8 shows the XRR result for the Hf(28 nm)/Ni(12 nm)/Hf(28 nm) film, which indicates that the thickness of the intermixing layer is slightly different between the top Ni/Hf and bottom Ni/Hf interfaces. These results suggest that the slight difference in the thickness of the intermixing layer does not strongly alter the interfacial orbital transparency T_{int} in the Hf/Ni/Hf trilayer.

-
- [1] K. Ando, S. Takahashi, K. Harii, K. Sasage, J. Ieda, S. Maekawa, and E. Saitoh, Electric manipulation of spin relaxation using the spin Hall effect, *Phys. Rev. Lett.* **101**, 036601 (2008).
- [2] A. R. Mellnik, J. S. Lee, A. Richardella, J. L. Grab, P. J. Mintun, M. H. Fischer, A. Vaezi, A. Manchon, E.-A. Kim, N. Samarth *et al.*, Spin-transfer torque generated by a topological insulator, *Nature (London)* **511**, 449 (2014).
- [3] J. Ryu, S. Lee, K.-J. Lee, and B.-G. Park, Current-induced spin-orbit torques for spintronic applications, *Adv. Mater.* **32**, 1907148 (2020).
- [4] L. Liu, C.-F. Pai, Y. Li, H. W. Tseng, D. C. Ralph, and R. A. Buhrman, Spin-torque switching with the giant spin Hall effect of tantalum, *Science* **336**, 555 (2012).
- [5] K. L. Wang, J. G. Alzate, and P. K. Amiri, Low-power non-volatile spintronic memory: STT-RAM and beyond, *J. Phys. D* **46**, 074003 (2013).
- [6] A. Hoffmann, Spin Hall effects in metals, *IEEE Trans. Magn.* **49**, 5172 (2013).
- [7] J. Sinova, S. O. Valenzuela, J. Wunderlich, C. H. Back, and T. Jungwirth, Spin Hall effects, *Rev. Mod. Phys.* **87**, 1213 (2015).
- [8] M. Tang, R. Ramaswamy, H. Yang, H. Yang, W. Fan, Z. Shi, S. Zhou, and X. Qiu, Ferromagnet structural tuning of interfacial symmetry breaking and spin Hall angle in ferromagnet/heavy metal bilayers, *Appl. Phys. Lett.* **113**, 222406 (2018).
- [9] H. Kontani, T. Tanaka, D. S. Hirashima, K. Yamada, and J. Inoue, Giant orbital Hall effect in transition metals: Origin of large spin and anomalous Hall effects, *Phys. Rev. Lett.* **102**, 016601 (2009).
- [10] D. Go, D. Jo, C. Kim, and H.-W. Lee, Intrinsic spin and orbital Hall effects from orbital texture, *Phys. Rev. Lett.* **121**, 086602 (2018).
- [11] D. Go and H.-W. Lee, Orbital torque: Torque generation by orbital current injection, *Phys. Rev. Res.* **2**, 013177 (2020).
- [12] D. Lee, D. Go, H.-J. Park, W. Jeong, H.-W. Ko, D. Yun, D. Jo, S. Lee, G. Go, J. H. Oh, K.-J. Kim, B.-G. Park, B.-C. Min, H. C. Koo, H.-W. Lee, O. Lee, and K.-J. Lee, Orbital torque in magnetic bilayers, *Nat. Commun.* **12**, 6710 (2021).
- [13] S. Lee, M.-G. Kang, D. Go, D. Kim, J.-H. Kang, T. Lee, G.-H. Lee, J. Kang, N. J. Lee, Y. Mokrousov, S. Kim, K.-J. Kim, K.-J. Lee, and B.-G. Park, Efficient conversion of orbital Hall current to spin current for spin-orbit torque switching, *Commun. Phys.* **4**, 234 (2021).
- [14] H. Hayashi, D. Jo, D. Go, T. Gao, S. Haku, Y. Mokrousov, H.-W. Lee, and K. Ando, Observation of long-range orbital transport and giant orbital torque, *Commun. Phys.* **6**, 32 (2023).
- [15] G. Sala and P. Gambardella, Giant orbital Hall effect and orbital-to-spin conversion in *3d*, *5d*, and *4f* metallic heterostructures, *Phys. Rev. Res.* **4**, 033037 (2022).
- [16] M. Taniguchi, H. Hayashi, N. Soya, and K. Ando, Nonlocal orbital torques in magnetic multilayers, *Appl. Phys. Express* **16**, 043001 (2023).
- [17] R. Fukunaga, S. Haku, H. Hayashi, and K. Ando, Orbital torque originating from orbital Hall effect in Zr, *Phys. Rev. Res.* **5**, 023054 (2023).
- [18] D. Jo, K.-H. Ko, D. Go, K.-H. Kim, H. G. Park, C. Kim, B.-C. Min, G.-M. Choi, and H.-W. Lee, Observation of the orbital Hall effect in a light metal Ti, *Nature (London)* **619**, 52 (2023).
- [19] A. Bose, F. Kammerbauer, R. Gupta, D. Go, Y. Mokrousov, G. Jakob, and M. Kläui, Detection of long-range orbital-Hall torques, *Phys. Rev. B* **107**, 134423 (2023).
- [20] D. Go, D. Jo, H.-W. Lee, M. Kläui, and Y. Mokrousov, Orbitoronics: Orbital currents in solids, *Europhys. Lett.* **135**, 37001 (2021).
- [21] J. Kim and Y. Otani, Orbital angular momentum for spintronics, *J. Magn. Magn. Mater.* **563**, 169974 (2022).
- [22] M.-H. Nguyen, D. C. Ralph, and R. A. Buhrman, Spin torque study of the spin Hall conductivity and spin diffusion length in platinum thin films with varying resistivity, *Phys. Rev. Lett.* **116**, 126601 (2016).
- [23] L. Liu, T. Moriyama, D. C. Ralph, and R. A. Buhrman, Spin-torque ferromagnetic resonance induced by the spin Hall effect, *Phys. Rev. Lett.* **106**, 036601 (2011).
- [24] D. Fang, H. Kurebayashi, J. Wunderlich, K. Výborný, L. P. Žárbo, R. P. Campion, A. Casiraghi, B. L. Gallagher, T. Jungwirth, and A. J. Ferguson, Spin-orbit-driven ferromagnetic resonance, *Nat. Nanotechnol.* **6**, 413 (2011).
- [25] V. Tshitoyan, C. Ciccirelli, A. P. Mihai, M. Ali, A. C. Irvine, T. A. Moore, T. Jungwirth, and A. J. Ferguson, Electrical manipulation of ferromagnetic NiFe by antiferromagnetic IrMn, *Phys. Rev. B* **92**, 214406 (2015).
- [26] T. Gao, A. Qaiumzadeh, H. An, A. Musha, Y. Kageyama, J. Shi, and K. Ando, Intrinsic spin-orbit torque arising from the Berry curvature in a metallic-magnet/Cu-oxide interface, *Phys. Rev. Lett.* **121**, 017202 (2018).
- [27] L. Salemi and P. M. Oppeneer, First-principles theory of intrinsic spin and orbital Hall and Nernst effects in metallic monoatomic crystals, *Phys. Rev. Mater.* **6**, 095001 (2022).
- [28] M. Akyol, G. Yu, J. G. Alzate, P. Upadhyaya, X. Li, K. L. Wong, A. Ekicibil, P. Khalili Amiri, and K. L. Wang, Current-induced spin-orbit torque switching of perpendicularly magnetized Hf[CoFeB]/MgO and Hf[CoFeB]/TaO_x structures, *Appl. Phys. Lett.* **106**, 162409 (2015).

- [29] M. Akyol, J. G. Alzate, G. Yu, P. Upadhyaya, K. L. Wong, A. Ekicibil, P. Khalili Amiri, and K. L. Wang, Effect of the oxide layer on current-induced spin-orbit torques in Hf[CoFeB]MgO and Hf[CoFeB]TaO_x structures, *Appl. Phys. Lett.* **106**, 032406 (2015).
- [30] R. Ramaswamy, X. Qiu, T. Dutta, S. D. Pollard, and H. Yang, Hf thickness dependence of spin-orbit torques in Hf/CoFeB/MgO heterostructures, *Appl. Phys. Lett.* **108**, 202406 (2016).
- [31] D. Go, F. Freimuth, J.-P. Hanke, F. Xue, O. Gomonay, K.-J. Lee, S. Blügel, P. M. Haney, H.-W. Lee, and Y. Mokrousov, Theory of current-induced angular momentum transfer dynamics in spin-orbit coupled systems, *Phys. Rev. Res.* **2**, 033401 (2020).
- [32] D. Go, D. Jo, K.-W. Kim, S. Lee, M.-G. Kang, B.-G. Park, S. Blügel, H.-W. Lee, and Y. Mokrousov, Long-range orbital torque by momentum-space hotspots, *Phys. Rev. Lett.* **130**, 246701 (2023).
- [33] L. Liao, F. Xue, L. Han, J. Kim, R. Zhang, L. Li, J. Liu, X. Kou, C. Song, F. Pan, and Y. Otani, Efficient orbital torque in polycrystalline ferromagnetic–metal/Ru/Al₂O₃ stacks: Theory and experiment, *Phys. Rev. B* **105**, 104434 (2022).
- [34] J. Liu, T. Ohkubo, S. Mitani, K. Hono, and M. Hayashi, Correlation between the spin Hall angle and the structural phases of early 5d transition metals, *Appl. Phys. Lett.* **107**, 232408 (2015).
- [35] B. D. Cullity, *Elements of X-ray Diffraction* (Addison-Wesley Publishing, Massachusetts, 1956).
- [36] U. Holzwarth and N. Gibson, The Scherrer equation versus the Debye-Scherrer equation, *Nat. Nanotechnol.* **6**, 534 (2011).
- [37] V. Uvarov and I. Popov, Metrological characterization of x-ray diffraction methods for determination of crystallite size in nano-scale materials, *Mater. Charact.* **58**, 883 (2007).
- [38] J. Kim, D. Go, H. Tsai, D. Jo, K. Kondou, H.-W. Lee, and Y. Otani, Nontrivial torque generation by orbital angular momentum injection in ferromagnetic-metal/Cu/Al₂O₃ trilayers, *Phys. Rev. B* **103**, L020407 (2021).